Visualisation of mechanisms governing suction bucket installation in dense sand

R. Ragni, B. Bienen, S.A. Stanier, M.J. Cassidy, C.D. O' Loughlin
Centre for Offshore Foundation Systems, 35 Stirling Hwy, Crawley, Perth, WA 6009 Australia

ABSTRACT: Suction buckets are an increasingly considered foundation option for offshore wind turbines. Although the required suction can be predicted well using existing methods, uncertainty remains around some input parameters, because the effects of suction installation on the soil state are not understood in detail. This paper visualises the mechanisms governing both initial self-weight penetration and following suction-assisted installation in dense sand. Pioneering particle image velocimetry measurements in a centrifuge environment underpinned the investigation, with details of the experimental apparatus offered in the paper. Changes in the deformation mechanisms governing the installation process and in the soil properties are revealed. The findings have an impact on the understanding of the formation of internal plug heave – the cause of premature refusal – and the prediction of the installation response. Revealing changes in void ratio and permeability also present implications on the accumulated displacements under the metocean loading, which may conflict with serviceability requirements.

1 INTRODUCTION

The suction bucket technology is nowadays regarded with interest for the foundations of offshore wind farms (Houlsby et al. 2005, Houlsby 2016), in relatively shallow waters. Associated with this application are more varied and coarser grained seabeds, requiring much stubbier suction buckets, and very different loading conditions when compared with traditional oil and gas applications (Tjelta 2015).

Suction buckets comprise a large diameter steel cylinder, open-ended at the bottom and closed at the top. In shallow water applications, typical aspect ratios are $L/D \leq 1$, where L is the skirt length and D is the bucket diameter, and $D/t = 100\sim250$, where t is the skirt thickness.

The first part of the installation is achieved under the self-weight of the bucket and substructure, with free flow of water through the vented bucket lid. When self-weight penetration is completed and a seal between the bucket and soil is established, the venting valve in the lid is closed and water is pumped from inside the bucket. This generates a differential pressure and a consequent additional downwards driving force in excess of the suction bucket submerged weight. In sand, the introduction of a suction-generated seepage field causes a reduction of the vertical effective stresses around the skirt tip, which reduces the vertical force required to install the bucket.

The initial self-weight penetration resembles other penetration processes, such as jacked installation of large diameter piles, although neglecting the vertical stress enhancement through the action of the downward friction has been flagged as non-conservative for the prediction of suction bucket installation (Houlsby & Byrne 2005). However, no guidance is provided on the size of this down-drag enhancement.

Suction-assisted penetration further induces changes in the soil state that are yet to be fully characterised, particularly in terms of variation in void ratio and permeability. Sound understanding, however, is crucial, as changes to the sand state considerably impact predictions. Loosening of the soil plug may result in premature refusal during suction bucket installation and adversely affect foundation performance in service.

This work presents particle image velocimetry measurements of suction bucket installation in dense sand, obtained in a centrifuge environment at enhanced gravity level. Insights into the self-weight and suction-assisted stages are provided, revealing changes in the deformation mechanisms and advancing fundamental understanding of the change of state of the sand plug.

2 EXPERIMENTAL SET-UP

2.1 *Centrifuge apparatus and arrangement*

The experiments presented in this paper were carried out in the geotechnical beam centrifuge at The

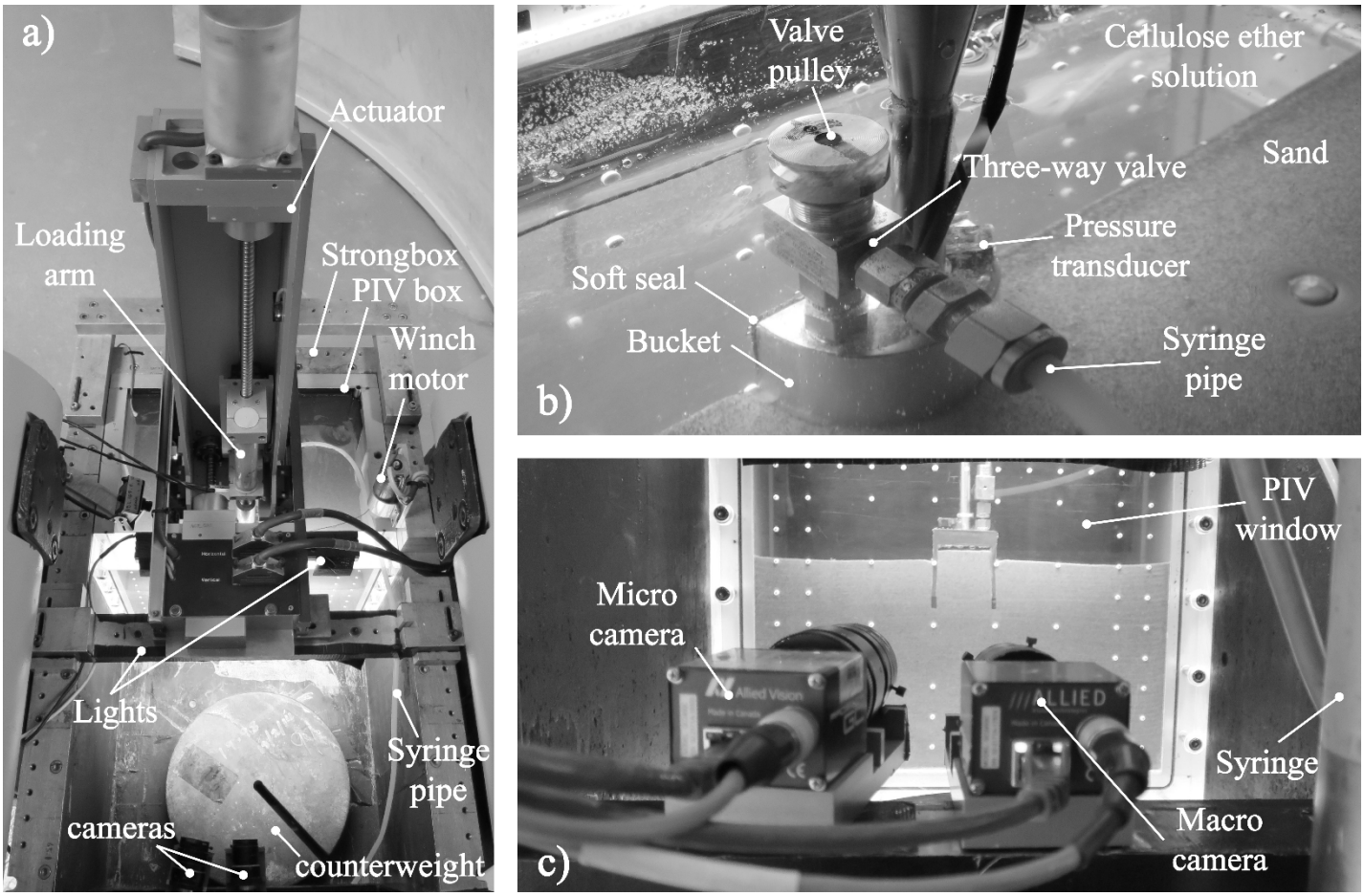

Figure 1: Illustration of the set-up for centrifuge testing.

University of Western Australia (Randolph et al. 1991), at an acceleration of 40 g. Particle Image Velocimetry (PIV) techniques (Stanier & White, 2013; Stanier et al. 2015) were used to reveal the failure mechanism associated with the suction bucket installation, where a half model of the foundation was penetrated against a Perspex window, and photographs of the event were captured.

An overview of the apparatus is presented in Figure 1a. A PIV box (inner dimensions 335×225×300 mm) containing the soil sample was housed in a larger sample container, termed 'strongbox'. The latter housed the remaining equipment; in particular, two cameras were placed opposite the PIV box, along with a 20 kg counterweight to limit the unbalance of the strongbox as it swung into position at 40 g. The bucket was connected to an electrically driven actuator using a steel shaft, and a 2 kN axial load cell was located between the bucket and the shaft. The actuator controlling the bucket motion was located on top of the strongbox. The actuator has two degrees of freedom: vertical, which was used to initially penetrate the bucket and control the bucket self-weight (via the axial load cell), and horizontal, which was used to position the bucket against the Perspex window. Two LED light panels provided sufficient lighting, such that the exposed face of the model was evenly and well illuminated. Finally, a winch and a syringe pump were fitted on the strongbox to control the fluid flow from the bucket (as described later).

The aluminium bucket model was designed with a skirt length $L = 50$ mm and outer diameter $D = 50$ mm (Fig. 2). This gives an aspect ratio $L/D = 1$, which is within the typical range and allowed PIV investigation of suction-assisted penetration over a significant depth. The skirt thickness t was 2 mm, such that $D/t = 25$, which although higher than employed for field scale buckets, was required to create an effective seal between the bucket and the window. Nonetheless, Tran (2005) demonstrated the skirt thickness to have a marginal effect on the penetration resistance during suction installation. A combination of soft sealant foam tape and hard rubber at the skirt tips was used at the bucket-window interface (Figs. 1b, 2), which was lubricated with petroleum jelly. This provided: (i) adequate sealing of the bucket interior from the external fluid; (ii) sufficient resistance against peeling of the foam tape during installation (enhanced by the hard rubber strips); and (iii) minimal friction generation during installation. The testing procedure required the fluid flow through the bucket lid to be: (i) directed to ambient; (ii) connected to the syringe pump; and (iii) stopped. This was achieved using a three-way valve placed on the lid top with a winch manipulating the valve configuration (Zhu et al. 2018). The valve was connected to the syringe pump via a flexible pipe. The bucket was equipped with a differential total pressure transducer

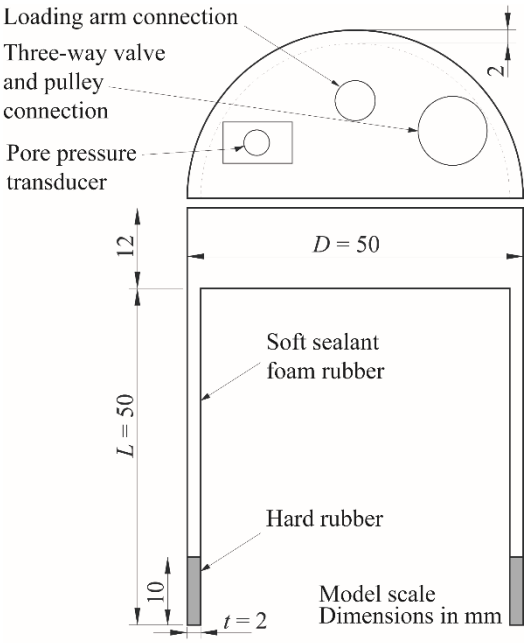

Figure 2: Schematic of the suction bucket model.

at the lid invert, which measured the suction pressure generated during installation.

Two 5-megapixel cameras mounted on a rigid crossbar captured images for the PIV analyses (Fig. 1c). The master macro-camera (8 mm lens) provided a view of the entire window, whereas the slave micro-camera (43 mm lens) focused on the region around the bucket tips, providing highly detailed images (at ~20 times the effective resolution of the macro camera) of this region of interest. The cameras captured images at a rate of 2 frame/s throughout the test. The thickness of the transparent window (50 mm) was estimated to limit lateral deflection of the window to less than 0.16 mm, which is sufficient to maintain approximately K_0 conditions following ramp-up to 40g (Haigh & Madabhushi 2014). An array of regularly spaced, pre-installed control markers inside the window was also required for the photogrammetric correction of the measurements. Further technical details regarding the dual camera arrangement and the lighting system can be found in Teng et al. (2017).

2.2 *Soil sample*

Commercially available fine silica sand (d_{50} = 0.18 mm) was used to prepare the sample. The sand properties are reported in Table 1 (after Chow et al. 2018). A fraction of the sand was dyed black in order to optimise the particle contrast as recommended in Stanier & White (2013) and then thoroughly mixed with the natural, white portion (75% natural, 25% black). A 175 mm high dense sample was achieved through dry pluviation of sand (including a more permeable 10-mm bottom layer of coarse sand separated by a layer of geotextile), following the procedure described in Xu (2007). Measurements of mass and volume of the sample confirmed a value of relative density D_r = 93%. The sample was then saturated from the base on the laboratory floor at 1 g with a solution of water and 1.1% cellulose ether content, to obtain a viscosity of 40cSt (DOV 2002). Matching the viscosity with the enhanced gravity level was necessary to correctly scale the drainage properties of the soil (Tan & Scott 1985, Taylor 1987, Dewoolkar et al. 1999). Throughout the centrifuge testing, a fluid head above the sample of 100 mm was maintained.

Table 1: Silica sand properties.

Specific gravity, *Gs*	2.67
Mean particle size, d_{50} [mm]	0.18
Minimum dry density, ρ_{min} [kg/m^3]	1497
Maximum dry density, ρ_{max} [kg/m^3]	1774
Critical state friction angle, ϕ'_{cv} [°]	31.6

Prior to the suction bucket tests, three cone penetration tests (CPTs) were carried out using a model scale cone penetrometer with a diameter of 10 mm at the testing acceleration of 40 g. These CPTs provided a basis for characterising each sample and to quantify potential density variations in and across the samples.

2.3 *Testing procedure*

The initial self-weight installation was modelled by penetrating the bucket vertically in displacement control, rather than under the self-weight of the foundation. This was necessary to ensure that the suction-assisted penetration initiated at the same bucket embedment depth in each test. A target normalised depth limited to z/L = 0.2 guaranteed a large portion of the skirt penetration to be investigated in suction-assisted regime. A constant rate of 0.057 mm/s was selected, as it is similar to the penetration rate measured in rigorous load-controlled self-weight penetration for full suction bucket tests reported in Bienen et al. (2018). At z/L = 0.2, the penetration resistance corresponded to a vertical force V = 82.5 N (at model scale), which was maintained constant during the subsequent suction-assisted penetration stage. The self-weight penetration was performed with the valve on the bucket lid set to 'vented', to allow fluid flow from the inside to the outside of the bucket as the foundation advanced into the soil.

After the bucket reached the targeted embedment depth, z/L = 0.2, the actuator was switched to load control to hold the vertical load previously achieved, and the winch motor was activated to connect the inner chamber of the suction bucket with the syringe pump. The syringe pump was then activated using a piston displacement rate of 0.06 mm/s, which resulted in a constant fluid flow of 117.8 mm^3/s being extracted from the bucket (at model scale). This is similar to the full suction bucket tests at the medium pumping flow rate in Bienen et al. (2018), which is typical of field conditions. This translates to a bucket penetration rate that reduces with time, since the seepage occurring below the skirt tips reduces the development of suction pressure. The pumping flow rate was maintained constant until full installation of the

bucket was reached (penetration was arrested immediately before the lid touched the surface to avoid sand plugging the fluid access port on the total pressure sensor or the three-way valve). The generation of suction was continuously monitored via the differential total pressure transducer located in the bucket lid.

3 PIV ANALYSIS

The PIV results presented in Figures 3-4 analysed a bucket penetration of $\Delta z = 1$ mm at different depths. For the generation of the contour plots, the measured displacement fields were normalised by the vertical displacement of the bucket $\Delta z = 1$ mm.

In contrast to the self-weight installation phase (Fig. 3), which was carried out at a constant penetration rate, the suction assisted stage (Fig. 4) involved a bucket penetration rate $\dot{z}$ that reduced with depth, as a steady pumping flow rate was maintained. The image acquisition rate was also kept constant at all times (2 frame/s).

GeoPIV-RG (Stanier et al. 2015) was used to analyse the image sequences recorded during the tests. The module relies on an array of subsets to analyse the soil domain, with the subset size and spacing of the subsets being user-defined. A subset size of 50 pixels was adopted here, equally spaced every 50 pixels (i.e. no subset overlap). The automatic reference image updating scheme was utilised in this work to track the soil displacements throughout the whole image series automatically whilst ensuring maximal correlations.

In general, modern image-based deformation algorithms can tolerate relatively large deformations (~10% strain), so long as the deformations are not overly localised (Stanier et al. 2016). In this work problems occurred at the surface of the sand plug due to localised piping, where the minimum correlation coefficient (CCZNCC) for a given image pair was less than the default criteria for GeoPIV-RG recommended by Stanier et al. (2015) (recommended CCZNCC $\geq$ 0.75; where 0 = no correlation and 1 = perfect correlation). Where these problems occurred, the analyses were concluded by relaxing the correlation coefficient criteria from the recommended values (from CCZNCC = 0.75 to 0.1 < CCZNCC < 0.5) before manually filtering all subsets from the analyses with a correlation coefficient < 0.75. This typically resulted in automated deletion of ~2% of the subsets analysed in a highly localised zone at the top of the sand plug.

4 RESULTS

The results presented here are part of a larger campaign investigating the effects of the variation of several key parameters. This paper focuses mainly on the experimental apparatus and the PIV analyses, reporting the results of a representative test only.

4.1 *Self-weight installation*

The resultant velocity contours for self-weight installation at $z/L = 0.195$ (PIV analysis of the preceding 1 mm penetration) are shown in Figure 3 (the dashed lines delimit the area captured by the micro-camera). The development of two independent mechanisms generated by the penetrating tips can be observed. The absence of overlapping at any point shows the lack of mutual influence.

Analogies with a penetrating strip footing (Houlsby & Byrne 2005) or cone (Senders & Randolph 2009) can be found. Bolton et al. (1999), defined a critical depth ($z/t \sim 10$) for a centrifuge scale CPT in sand, which is the depth at which the behaviour transitions from shallow to deep. In this sense, the response displayed in Figure 3 aligns with the prediction of shallow foundation behaviour expected at $z/t \sim 5$.

However, asymmetry of the failure mechanism under each skirt is apparent. In order to understand the reason behind this, changes in soil stresses generated by skirt friction are examined. Houlsby & Byrne (2005) suggested that the penetration-generated friction increases the vertical effective stress around the skirt, and consequently also the tip resistance. This down-drag effect is expected to be more pronounced on the inside of the bucket compared to the outside, leading to a shift in vertical stresses at the skirt tip from a symmetric (under equal conditions inside and outside of the bucket) towards an asymmetric stress distribution, with consequences for the symmetry of the mechanism. Similar changes in soil stresses have been reported for jacked piles in Henke & Bienen (2014). The effect of changes in soil stress induced by the advancing skirts is evident in Figure 3, where the mechanism under the skirt tip has shifted outside the bucket, and now consequently extends to the soil surface at different gradients inside compared to outside of the bucket.

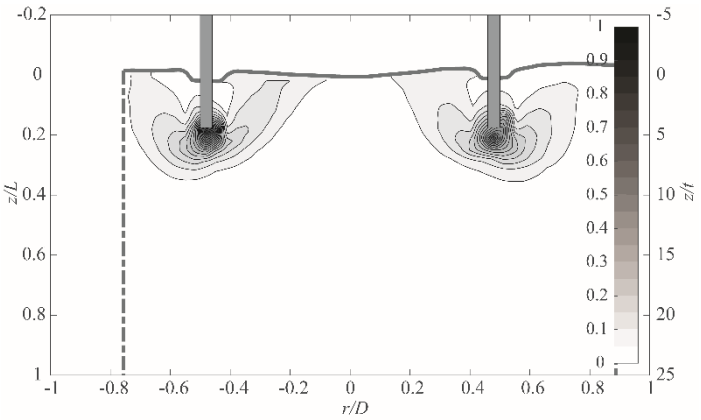

Figure 3: Normalised resultant velocity contours at the end of self-weight installation ($z/L = 0.2$).

4.2 *Suction-assisted installation*

Figure 4 shows the normalised resultant velocity contours at increasing normalised depths: z/L = 0.38; 0.56; 0.74. In contrast to Figure 3, overlapping of the mechanisms originating from each tip is now apparent. In fact, a single mechanism now characterises the process.

The mechanism shows marked changes compared to that under self-weight (jacked) penetration. The mechanism under the skirt tip has shifted to concentrate inside the bucket. The prevalent inwards and upwards flow of soil observed inside the bucket contrasts with the extremely limited downwards motion outside, which is simply generated by the skin friction.

The generation of suction is responsible for the seepage field established inside and outside the bucket, with seepage patterns that have been extensively investigated numerically (Erbrich & Tjelta 1999, Tran 2005, Senders 2008). The high velocity observed around the bucket tips in Figure 4, along with the upwards movement of the internal soil, is consistent with steep upwards hydraulic gradients generated by the suction. Furthermore, they are consistent with the theory that resistance in suction installation is reduced through reduction of effective vertical stresses around the skirt tip. Further, the lack of any soil movement outside the bucket is consistent with the theory of low hydraulic gradients in this region (Senders & Randolph 2009).

As the bucket advances into the soil as a consequence of the increasing suction, Figure 4 shows that the shape of the failure mechanism remains largely unaffected; it simply moves with the penetrating bucket. The rate at which the plug moves upwards appears to be a constant fraction of the bucket penetration rate (as a reducing penetration rate $\dot{z}$ also involves the plug moving more slowly). The prevalent upwards mobilisation of the soil can be associated with the inner seepage flow. The gradual formation of soil plug heave led to a final recorded value of ~0.15 L above the original soil surface, which is close to the volume of soil displaced by the skirts (quantified in 0.136 L). According to Figure 4 (and to the vector plots not included here) it is reasonable to assume that all the soil displaced by the penetrating skirts entered the bucket. It can then be estimated that the skirt penetration is the main cause of the plug heave observed (~90%), with seepage-triggered sand dilation only partially responsible (~10%). Dilation caused by shearing of the dense sand along the skirts (Tran et al. 2005) does not appear to have a particular influence on the plug heave formation.

Critical hydraulic gradients are thought to have occurred around the tips and within the soil plug. However, the consequent changes in soil state are not uniform across the plug, as localised singularities of

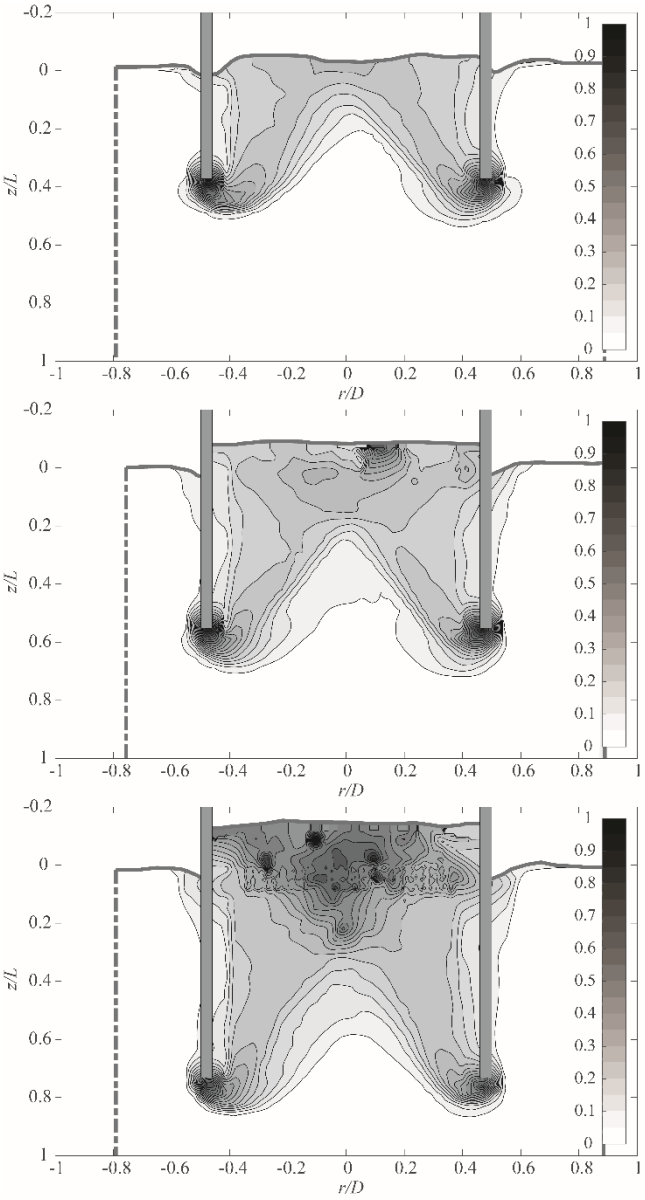

Figure 4: Normalised resultant velocity contours at (a) z/L = 0.18; (b) z/L = 0.36; (c) z/L = 0.54

large soil displacement can be observed in its uppermost part in Figure 4c. In contrast to the tips, the sand close to the surface is not confined, so that localised phenomena of piping, associated with negative pressures above the critical value and localised high-velocity regions were captured. It should be clarified that, as piping occurs, it becomes increasingly complex for PIV analysis to track the particle displacement (see Section 3), for this is associated with extremely rapid velocities and highly localised deformations. The finding that plug heave formation is mainly a consequence of skirt penetration, along with the observation of these localisations only towards the final stage of suction installation, would suggest that only a minor increase in void ratio, and thus soil permeability, took place in the soil plug. However, further study on the measured volumetric strain is required to accurately determine the changes in void ratio.

5 CONCLUDING REMARKS

The Particle Image Velocimetry (PIV) technique was successfully applied to the problem of suction bucket installation in a centrifuge environment. Velocity contours revealed substantial differences between the mechanisms governing the initial self-weight installation and the subsequent suction stage. The effect of down-drag enhancement of soil stresses due to friction on the suction bucket skirt was observed during the self-weight penetration phase. The analyses revealed the mechanism during suction-assisted penetration to consist of shearing, and confined within the bucket. Non-uniform positive volume change within the soil plug was associated with events of localised piping. Minimal soil displacement was generated by the friction along the external skirt face.

The PIV centrifuge experiment discussed in this paper forms part of a larger testing programme, which aims to explore the effects of the bucket diameter (and hence confining conditions), the initial sand relative density and the pumping flow rate on the soil response.

6 ACKNOWLEDGEMENTS

This work forms part of the activities of the Centre for Offshore Foundation Systems (COFS), which is currently supported as one of the primary nodes of the Australian Research Council (ARC) Centre of Excellence for Geotechnical Science and Engineering and as a Centre of Excellence by the Lloyd's Register Foundation. Lloyd's Register Foundation helps to protect life and property by supporting engineering-related education, public engagement and the application of research. The third author is supported by an ARC DECRA Fellowship. This support is gratefully acknowledged.

REFERENCES

Andersen, K.H., Jostad, H.P. & Dyvik, R. 2008. Penetration resistance of offshore skirted foundations and anchors in dense sand. *Journal of geotechnical and geoenvironmental engineering* 134(1): 106-116.

Bienen, B., Klinkvort, R.T., O'Loughlin, C.D., Zhu, F. & Byrne, B.W. 2018. Suction buckets in dense sand: Installation, limiting capacity and drainage. *Géotechnique* https://doi.org/10.1680/jgeot.16.p.281

Bolton, M.D., Gui, M.W., Garnier, J., Corte, J.F., Bagge, G., Laue, J. & Renzi, R. 1999. Centrifuge cone penetration tests in sand. *Géotechnique* 49(4): 543-552.

Chow, S.H., O'Loughlin, C.D., Gaudin, C. & Lieng, J.T. 2018. Drained monotonic and cyclic capacity of a dynamically installed plate anchor in sand. *Ocean Engineering* 148: 588-601.

Dewoolkar, M.M., Ko, H.Y., Stadler, A.T. & Astaneh, S.M.F. 1999. A substitute pore fluid for seismic centrifuge modeling. *Geotechnical Testing Journal* 22(3): 196-210.

DOV 2002. Methocel Cellulose ethers. *Technical Handbook*.

Haigh, S.K. & Madabhushi, S.P.G. 2014. Discussion of "Performance of a transparent flexible shear beam container for geotechnical centrifuge modelling of dynamic problems by Ghayoomi, Dashti and McCartney". *Soil Dynamics and Earthquake Engineering* 67: 359-362.

Henke, S. & Bienen, B. 2014. Investigation of the influence of the installation method on the soil plugging behaviour of a tabular pile. *In Proc. International Conference on Physical Modelling in Geotechnics, Perth, Australia*: 14-19.

Houlsby, G.T. & Byrne, B.W. 2005. Design procedures for installation of suction buckets in sand. *In Proc. of the Institution of Civil Engineers-Geotechnical Engineering* 158(3): 135-144.

Houlsby, G.T., Ibsen, L.B. & Byrne, B.W. 2005. Suction buckets for wind turbines. *In Proc. International Symposium Frontiers in Offshore Geotechnics, Perth, Australia:* 75-93.

Houlsby, G.T. 2016. Interactions in offshore foundation design. *Géotechnique* 66(10): 791-825.

Randolph, M.F., Jewell, R.J., Stone, K.J.L. & Brown, T.A. 1991. Establishing a new centrifuge facility. *In Proc. International Conference Centrifuge, Boulder, USA: 3–9.*

Senders, M. 2008. Suction buckets in sand as tripod foundations for offshore wind turbines. *PhD thesis, The University of Western Australia, Australia*.

Senders, M. & Randolph, M.F. 2009. CPT-based method for the installation of suction buckets in sand. *Journal of Geotechnical and Geoenvironmental engineering* 135(1): 14-25.

Stanier, S.A. & White, D.J. 2013. Improved Image-Based Deformation Measurement in the Centrifuge Environment. *Geotechnical Testing Journal* 36(6): 915-928

Stanier, S.A., Blaber, J., Take, W.A. & White, D.J. 2015. Improved Image-Based Deformation Measurement for Geotechnical Applications. *Canadian Geotechnical Journal* 53(5): 727-739.

Stanier, S.A., Dijkstra, J., Leśniewska, D., Hambleton, J., White, D.J. & Wood, D.M. 2016. Vermiculate artefacts in image analysis of granular materials. *Computers and Geotechnics* 72: 100-113.

Tan, T.S. & Scott, R.F. 1985. Centrifuge scaling considerations for fluid-particle systems. *Géotechnique*, *35*(4): 461-470.

Taylor, R.N. 1987. Discussion of "Tan, T.S. and Scott, R.F. (1985). Centrifuge scaling considerations for fluid-particle systems." *Géotechnique* 37(1): 131-133.

Teng, Y., Stanier, S.A. & Gourvenec, S.M. 2017. Synchronised multi-scale image analysis of soil deformations. *International Journal of Physical Modelling in Geotechnics* 17(1): 53-71.

Tjelta, T.I. 1990. The Skirt piled Gullfaks C installation. *In Proc. Offshore Technology Conference, Houston, USA*.

Tjelta, T.I. 2015. The suction foundation technology. *In Proc. International Symposium Frontiers in Offshore Geotechnics, Oslo, Norway:* 85-93.

Tran, M.N. 2005. Installation of suction buckets in dense sand and the influence of silt and cemented layers. *PhD thesis, The University of Sydney, Australia*.

Tran, M.N., Randolph, M.F. & Airey, D.W. 2005. Study of sand heave formation in suction buckets using Particle Image Velocimetry (PIV). In *Proc. International Symposium Frontiers in Offshore Geotechnics, Perth, Australia:* 259-265.

Tran, M.N. & Randolph, M.F. 2008. Variation of suction pressure during bucket installation in sand. *Géotechnique*, 58(1): 1-11.

Xu, X. 2007. Investigation of the end bearing performance of displacement piles in sand. *PhD thesis, The University of Western Australia, Australia.*

Zhu, F., Bienen, B., O'Loughlin, C.D., Cassidy, M.J. & Morgan, N. 2018. Suction caisson foundations for offshore wind energy: installation and cyclic response in sand and sand over clay. *Géotechnique, under review.*

View publication stats